EASR

Engineering and Applied Science Research

https://www.tci-thaijo.org/index.php/easr/index

Published by the Faculty of Engineering, Khon Kaen University, Thailand

Performance analysis of combined cycle power plant inlet air cooling by a novel optimized vapour absorption refrigeration framework

Mude Murali Mohan Naik*[1)], V.S.S. Murthy[2)] and Bandaru Durga Prasad[1)]

[1)]Department of Mechanical Engineering, JNTUA College of Engineering, Anantapuramu, Andhra Pradesh - 515002, India
[2)]Department of Mechanical Engineering, KSRM College of Engineering, Kadapa, Andhra Pradesh - 516003, India

Received 27 January 2023
Revised 2 May 2023
Accepted 31 May 2023

Abstract

A Combined Cycle Power Plant (CCPP) is utilized for generating electricity, and it is a highly effective, efficient generation unit of power. However, heat absorbance maximization has played a significant role in CCPP applications. The heat absorbance system has recorded less heat absorbance rate in many cases. Hence, the present research is focused on CCPP with Heat Recovery Steam Generator (HRSG) and Vapour Absorption-based Refrigeration (VAR) cooling system based on Lithium Bromide-Water ($LiBr/H_2O$). Furthermore, the thermodynamic model for the air cooler and the integrated system was analyzed. Moreover, a novel Hybrid Ant Colony Bat Absorber system (HACBAS) was developed to optimize heat absorbance and energy. This process has maximized the Coefficient of Performance (COP) of the absorbance to the desired level. The CCPP absorption system simulation model is carried out with the MATLAB platform. In addition, the presented model has gained the optimized COP as 0.97%, and the gained energy efficiency is 95%. Also, the recorded generation by the designed model is 943MW. Hence, the presented optimal solution is suitable for the CCPP applications to optimize the heat absorbance rate and maximize energy efficiency.

Keywords: Combined cycle power plant, Heat recovery steam generator, Vapor absorption-based refrigeration cooling system, Optimized absorber system, Lithium bromide-water

1. Introduction

Thermal engineering [1] converts heat energy into chemical, mechanical, and electrical power [2]. Thermal management is essential to avoid the failure of components; thermal radiation may affect workers' health [3]. Thermal engineering is used in various applications such as combustion engines, thermal insulation, solar heating, heat exchangers, boiler design, and cooling systems [4]. Thermal engineering is mainly based on thermodynamics concepts [5]. Thermodynamics is the storage, transfer, and conversion of energy. Heat conduction means transferring heat from one body to another by contact [6]. The CCPS architecture is detailed in Figure 1.

Thermal radiation is an exchange of heat by electromagnetic radiation. Also, there is no need for two bodies to contact each other [7]. The primary application of thermal engineering is power plants, refrigeration, refineries, chemical processing, food processing, and preservation units [8]. Recently, many techniques have been processed to improve the inlet cooling method, reduce heat wastage, and improve thermal efficiency [9]. Many researchers try to solve the problem in a variety of ways hybrid turbine by inlet air cooling (TIAC) system, Brayton Rankine Combined-cycle power plant (CCPP) [10], ORC-ARS system, etc., [11]. Several vapour absorption models were implemented in the past, but those models have attained less thermal efficiency range. The inlet air cooling system was introduced in the CCPP model [12]. Two thermodynamic cycles of the Steam and gas turbine cycle combine to form the CCPP [13]. Two processes complement each other to create an efficient combined power cycle [14]. High-temperature resource requires for the Brayton cycle, and a high-temperature discharge source is used for the Rankine cycle [15].

Two main types of inlet air cooling methods are 1) Water evaporation and 2) Heat transfer systems. Water evaporation involves inlet fogging and evaporative cooling; the temperature will decrease directly [16]. The heat transfer system lowers air temperature indirectly to the power plant situated area, weather conditions, etc., [17]. Power generation and CCPPs depend on gas turbines. Moreover, the cost is less, the compact size, the flexibility of fuel, lightweight, and low emissions [18].

Moreover, several works have been done in the past, like Hybrid sorption-vapor, compression cooling systems [19], Reuse of heat wastage [20], Integrated Cooling systems with CCPP [21], etc. But still, there is no improvement in increased heat absorbance. Numerous research works include energetic optimization for CCPP to maximize energy and exergy efficiencies. However, it has recorded a poor heat absorption rate. So, Fakhari et al. [22] have designed an optimization model for the CCPP that has included three objective functions, which have regulated the heat absorbance rate and energy efficiency. However, a high error rate has been attained.

*Corresponding author.
Email address: mudemuralimohannaik92@gmail.com
doi: 10.14456/easr.2023.33

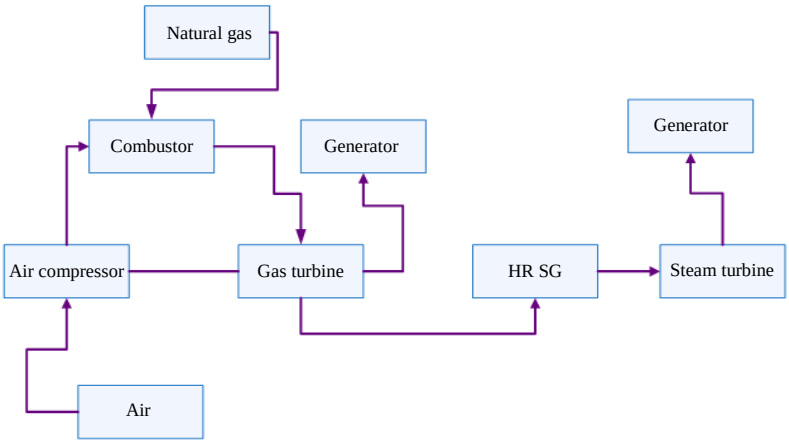

Figure 1 Combined cycle power plant

Moreover, Miah et al. [23] have modelled the CCPP based on two fuels. Hence, it has gained the finest energy efficiency score. However, high emission rates and high economic costs have been recorded. Wan et al. [24] have introduced an economic analysis model and heat recycling system to reduce heat energy wastage. Here, the excess heat has been taken as the input inlet of the cooling system. Hence, this system has a high cooling capacity range but is reported in low power generation.

Hence, the research gaps have described that some models were inefficient in power generation, and some recorded poor heat absorbance rates. In addition, few schemes have recorded a high error rate. So, the optimized heat absorbance rate has been designed for the CCPP system. Here, the key novelty of this research work is implementing the hybrid optimization model based on ant and bat functions to tune the CCPP parameters to gain better efficiency and COP. The key contribution of this research work is described below:

- The combined power plant was initially designed in the MATLAB/SIMULINK environment.
- Consequently, a novel HACBAS was designed to tune the absorber performance to optimize the absorber performance.
- The designed model was tested for different climate conditions.
- Hereafter, Social impacts are analyzed for the designed combined plant refrigeration model.
- Subsequently, a comparison has been made to know the percentage of improvement of the present model over the old techniques in terms of resource economics and energy consumption.

The paper structure is described as follows: the recent literature related to the CCPP is discussed along with the problems in the related work section. The proposed section explains the proposed methodology and its process, the outcome of the presented work are defined in results and discussion section, and conclusion section has ended the research discussions.

2. Related works

Some of the possible literature associated with a CCPP by inlet air cooling and vapor absorption in a refrigeration system is summarized below:

Gado et al. [19] have analyzed a Hybrid absorption-vapour and compression cooling system. The heat from the condenser is sent into absorption and adsorption chillers. A significant amount of heat is given to the desorber; therefore, there is no need to direct heat to the chillers. The main advantage is accurate temperature with high-speed response, suitable for humid and hot temperatures. The main disadvantage is the large size, lack of moving parts, and more time to introduce into the market.

Organic Rankine Cycle (ORC) is used for generating power from the diesel engine's waste heat energy, used for refrigeration by absorption-based refrigeration system (ARS) and the adsorption-based cooling system (ACS). Alklaibi and Lior [20] proposed ORC is utilized for power generation and refrigeration systems. Fuel consumption is reduced by 5-11.3%, and thermal efficiency is increased by up to 5%. ORC-ARS system improved by 3% heat recovery.

To meet the high peak load in summer, Fakhari et al. [22] have analyzed combined energy and heat for the power plant by inlet cooling absorption and evaporative after cooling. In a combustion chamber, heat recovery steam generator, and generative heat exchanger, it is reported that most of the destruction cycles are happening. The overall efficiency and ratio are influenced by the cycle's energy efficiency and power-to-heat ratio—75% of exergy destruction during the combustion.

Peng and Sadaghiani [21] introduced Integrated Cooling System with CCPP to reduce the water temperature from the condenser. ORC is connected to the Hellen cooling tower to improve the cooling capacity. This method can decrease water temperature from 313K to 303K. This method can improve the cooling ability of the Hellen Tower. The stability of the cooling system generates more power. The exergy efficiency rate is 37.59%. This parameter increases from 20.04% to 21.94%, and optimizing the system increases capital costs.

Ahmad et al. [25] have analyzed the integration of hybrid inlet cooling & solar systems. The flue gas produces energy from the CCPP combined with a power generator. Flue gas from the gas turbine directed to the heat recovery generator increases the temperature, where flow is separated into a stream. By this method, power is increased up to 22.8% and efficiency by 4.3%, and fuel consumption decreases by 8.4%. Capital cost is high.

2.1. System model and problem description

The combined cycle power plant (CCPP) system has attracted many researchers because of its advances in both ways, which are electricity production and cooling capacity. CCPP has both steam and gas turbines for network power supply. The system model of the CCPP is represented in Figure 2.

The steam and gas turbine (GT) was utilized in CCPP for electricity production. The gas turbine is used for air compression and fuel mixing; the steam turbine converts the high-velocity energy produced by steam into mechanical energy. Moreover, the steam turbine (ST) and generator are combined to transform the turbine's mechanical energy into electricity. However, the poor absorber can maximize power usage by absorbing excess power. The CCPS has attained poor electricity production and cooling performance in that case. Where HP represents the high pressure; LP is low pressure; HT is the high temperature; LT means the low temperature; GT indicates the gas turbine; ST represents the steam turbine; RH is the re-heater; SH is the superheater; EVAP denotes the evaporator; eco is defined for economizer; CPH is characterized for condensate preheater; FP is the feed pump; CEP is the condensate extraction pumps.

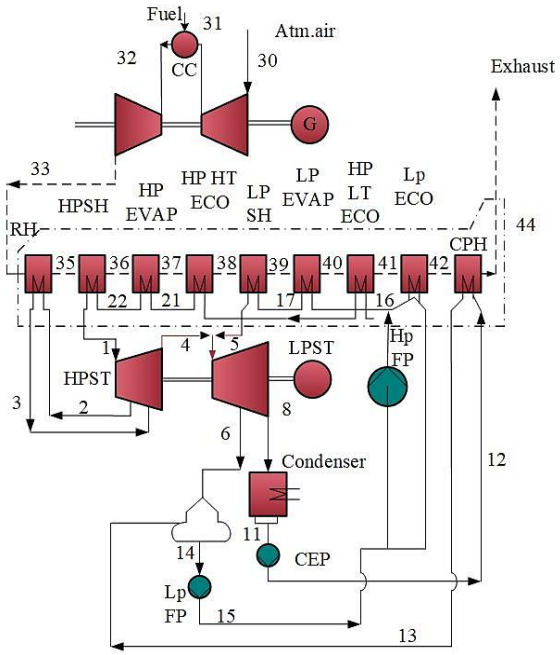

Figure 2 System model

3. Proposed Hybrid Ant Colony Bat Absorber System (HACBAS)

To optimize the heat absorber to attain the best cooling capacity and electricity-producing level, the present article has aimed to design a novel hybrid optimization strategy known as the Hybrid Ant Colony Bat Absorber System (HACBAS). The required amount of heat is taken for cooling purposes, and other waste heat is utilized to produce electricity by implementing the proposed methodology. The proposed architecture is detailed in Figure 3.

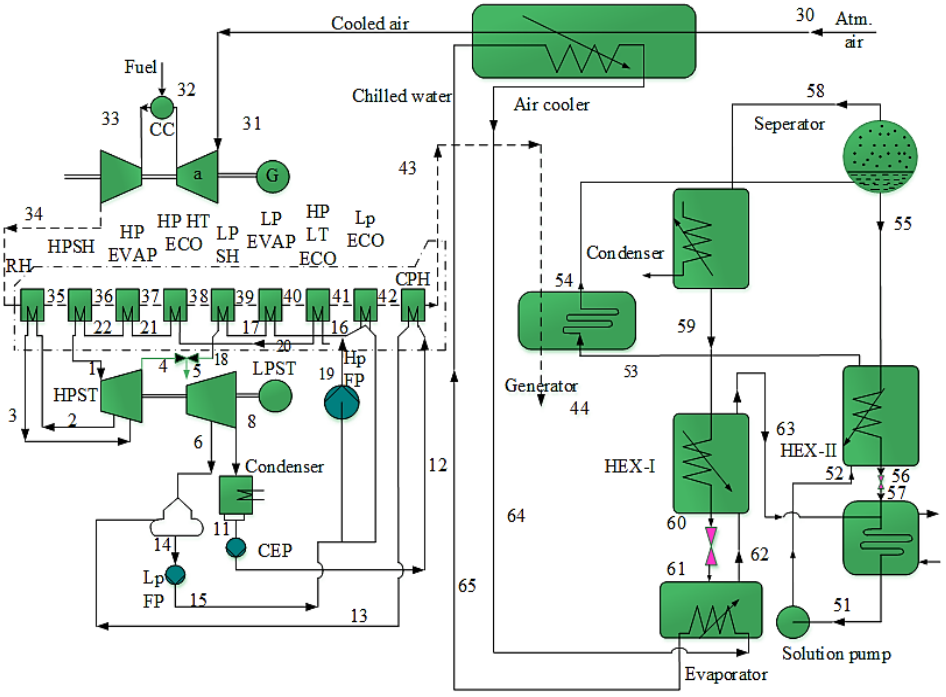

Figure 3 proposed methodology

Where a: HACBAS, HRSG represents the heat recovery steam generator, and HEX is the heat exchanger. In CCPP, the primary purpose of HRSG is to recover the heat from the GT hot gases to generate steam for the ST. The HRSG contains four components, i.e., a superheater, water preheater, evaporator, and economizer. Moreover, it is categorized into multi-pressure or single-pressure based on the pressure levels. Here multi (dual) pressure is utilized in the proposed HRSG.

3.1 Thermodynamic model of air Cooling and integrated power system

In the presented CCPP model, the GT plant is provided at the top of the power plant, and the ST plant is supplied at the bottom. These two plants were coupled with an HRSG with dual-based pressure. To obtain the gas and steam's minimum difference in temperature, the HRSG's heating devices are arranged. To cool the inlet air-based cooling of the compressor, Lithium Bromide (LiBr)/water (H2O) in a single effect Vapour absorption-based Refrigeration (VAR) system was provided. To decrease the atmospheric temperature of the air, the cooling system evaporator is combined with an air cooler. The chilled water circuit was placed between the air cooler and evaporator heat exchangers to transfer the heat from the cooling coil to the air. The heat recovery system provides power to the VAR-based cooling system in the plant sack. It works as a lower-grade thermal energy source for supplying cooling systems about 80^0C-100^0C. For a simple gas cycle, the ambient temperature of GT in the inlet is 30^0C, and 14^0C-30^0C is taken as the air temperature of GT with a VAR-based cooling system.

The GT and compressor isentropic efficiency are evaluated from the pressure ratio, expressed in Eqn. (1) & Eqn. (2).

GT's isentropic efficiency, $$\delta_{GT} = \frac{1-\left(\frac{S_{33}}{S_{32}}\right)^{\frac{\delta_{\infty GT}(\tau-1)}{\tau}}}{1-\left(\frac{S_{33}}{S_{32}}\right)^{\frac{(\tau-1)}{\tau}}} \quad (1)$$

Compressor's isentropic efficiency, $$\delta_C = \frac{P_r^{\left(\frac{\tau-1}{\tau\delta_{\infty C}}\right)}-1}{P_r^{\left(\frac{\tau-1}{\tau}\right)}-1} \quad (2)$$

Where, δ_{GT} and δ_C represents the GT and compressor isentropic efficiency respectively, P_r denotes the pressure ratio, S denotes the isentropic relation, δ_∞ represents the efficiency of isentropic state, τ represents the ratio of specific heat, $\delta_{\infty GT}$ and $\delta_{\infty C}$ denotes the isentropic efficiencies of GT and compressor respectively. The modelling of the CC system was started with a selected deaerator-based pressure. The saturated liquid is an existing state of the deaerator, and from the saturation temperature, the LP is determined. Heat balance equations determine the heating devices of steam's flow rate and gas temperature. The LP evaporator saturation temperature is evaluated using Eqn. (3),

$$ST^*_{LP} = T^*_{LPexit} - DSH_{LP} - TTD_{LP} \quad (3)$$

The flue gas outlet temperature at HP evaporator, $T^*_{36} = ST^*_{HP} + PP_{HP}$ (4)

The flue gas outlet temperature at LP evaporator, $T^*_{39} = ST^*_{LP} + PP_{LP}$ (5)

The water outlet temperature at HP, HT economizer, $T^*_{21} = ST^*_{HP} - AP_{HP}$ (6)

The outlet temperature of water at LP economizer, $T^*_{16} = ST^*_{LP} - AP_{LP}$ (7)

Where, ST represent the saturation temperature. The interaction of works in steam and gas cycles is computed to fuel unit mass. For exergy analysis, the irreversibility in all the components is estimated to measure the energetic losses. This analysis evaluates the failures and efficiency of fuel with 1kmol. The maxima of fuel exergy and chemical availability were attained in theoretical work by allowing the energy to correlate with environment-based oxygen to generate the water vapor and carbon dioxide environmental components. The chemical contribution plays a vital role in the gas combustor based on fuel, and the component's chemical exergy is evaluated for each state by Eqn. (9).

Chemical exergy, $E_{ch} = \sum_m n_m \varepsilon_m^0 + RT^*_0 \sum_m n_m \ln\left[Px_m\right]$ (8)

Where, m^{th} components mole fraction is denoted as x_m, R denotes reheat, and the physical exergy of components is determined by Eqn. (9),

Physical exergy, $E_{ph} = h - \sum_m T^*_0 s_m$ (9)

Total exergy, $E = E_{ch} + E_{ph}$ (10)

The thermally operated LiBr/H_2O cooling system evaluations are presented below. The circulation ratio is determined using Eqn. (11),

$$\delta = \frac{m^*_s}{m^*_r} = \frac{x_w}{x_s - x_w} \tag{11}$$

$$\Rightarrow \frac{m^*_{55}}{m^*_{61}} = \frac{x_{54}}{x_{55} - x_{54}} \tag{12}$$

Where, m^*_s represents the mass of strong solution, m^*_r denotes the mass of refrigerant, x_w and x_s denotes the concentration of the weak and strong solution, respectively. At the absorber, the mass of weak solution is computed using Eqn. (13),

$$m^*_w = m^*_s + m^*_r \tag{13}$$

i.e., $m^*_{51} = m^*_{57} + m^*_{63}$ (14)

If, m^*_w = 1kg/s, then,

$$m^*_r = \frac{m^*_w}{1+\delta} \tag{15}$$

From the exit temperature of HRSG, the separator temperature $\left(T_{54}\right)$ is determined by Eqn. (16),

$$T^*_{54} = T^*_{43} - AP \tag{16}$$

The working fluid temperature before throttling is evaluated by Eqn. (17),

$$T^*_{56} = T^*_{52} + AP \tag{17}$$

The HEX II energy balance is determined by Eqn. (18),

$$h^*_{53} = h^*_{52} + \frac{m^*_{55}(h^*_{55} - h^*_{56})}{m^*_{53}} \tag{18}$$

The concentration of weak solution from generators energy is evaluated by Eqn. (19),

$$m^*_{53} = \frac{m^*_{gas}(h^*_{43} - h^*_{44})}{(h^*_{54} - h^*_{53})} \tag{19}$$

The equation of energy balance between the evaporator and air cooler is given in Eqn. (20),

$$h_{31}^{*} = h_{30}^{*} - \frac{m_{61}^{*}(h_{62}^{*} - h_{61}^{*})}{m_{air}^{*}} \tag{20}$$

Eqn. (21) determines the required chilled water mass. The evaporator's refrigerant mass is computed by Eqn. (22),

$$m_{cw}^{*} = \frac{m_{air}^{*}(h_{30}^{*} - h_{31}^{*})}{P_{c,cw}(T_{64}^{*} - T_{65}^{*})} \tag{21}$$

$$\overset{\circ}{m}_{r}^{*} = \frac{m_{cw}P_{c,cw}(\overset{\circ}{T}_{64}^{*} - T_{65}^{*})}{(h_{62}^{*} - h_{61}^{*})} \Rightarrow \frac{m_{a}(\overset{\circ}{h}_{30}^{*} - h_{31}^{*})}{(h_{62}^{*} - h_{61}^{*})} \tag{22}$$

After the generated vapor, the exhaust temperature of gas T_{44}^{*} can be evaluated from h_{44}^{*} in Eqn. (23),

$$h_{44}^{*} = h_{43}^{*} - \frac{m_{w}^{*}(h_{54}^{*} - h_{53}^{*})}{m_{e}^{*}} \tag{23}$$

Where, m_{e}^{*} represents the mass of exhaust gas, m_{cw}^{*} denotes the mass of chilled water, and m_{air}^{*} is the mass of air.

3.2 Process of HACBAS

The HACBAS was proposed to optimize the heat absorber in CCPP to attain the best electricity-producing level and cooling capacity. In this research, the novel framework was designed with the combination of Ant Colony [26] optimization (ACO) and Bat optimization (BO) [27]. The ant developed a path between the food source and its colony in ACO. The distance of the path is estimated through pheromone trails, which were randomly left from the ant movements. Moreover, in this research, ACO was utilized for energy optimization. Consequently, the bat produces a sound in BO to locate their food. In this research, BO absorbs heat to increase the electricity-producing level. In the initial stage process of the probability, stage construction is expressed in Eqn. (24),

$$R_{k,l}^{*} = \frac{\left(m_{k,l}^{\alpha}\right)\left(w_{k,l}^{\beta}\right)}{\Sigma\left(m_{k,l}^{\alpha}\right)\left(w_{k,l}^{\beta}\right)} \tag{24}$$

Where, $m_{k,l}$ represents the amount of energy on k,l^{th} components, α denotes the parameter to control the energy $m_{k,l}$ influence, $w_{k,l}$ is the desired energy of k,l^{th} components and β denotes the parameter to control the desired energy $w_{k,l}$ influence. Eqn updates the amount of energy. (25),

$$m_{k,l} = (1-\delta)m_{k,l} + \Delta m_{k,l} \tag{25}$$

Where, δ is the rate of energy evaporated, $\Delta m_{k,l}$ represents the amount of energy deposited, typically given using Eqn. (26),

$$\Delta m_{k,l}^{x} = \begin{cases} 1/Q_{x} & if \quad energy \quad distributed\ on \quad k,l^{th} components \\ 0 & otherwise \end{cases} \tag{26}$$

Where, Q_x is the x^{th} components energy cost (typically length). Moreover, the fitness of BO is added to ACO fitness for enhancing the fitness function. The fitness of the bat's movement is expressed by Eqn. (27),

$$H_{a} = H_{\min} + \left(H_{\max} - H_{\min}\right)\alpha \tag{27}$$

$$\Rightarrow m_{k}^{t+1} = m_{k}^{t} + \left(y_{k}^{t} - y^{*}\right)H_{a} \tag{28}$$

$$\Rightarrow y_{k}^{t+1} = y_{k}^{t} + m_{k}^{t} \tag{29}$$

Where, $\alpha \in (0,1)$ denotes the random vector, y^* represents the best heat absorber components among all the components at each iteration t. H_a is the heat absorber velocity increment. In this implementation, we use $H_{\min} = 0$ and $H_{\max} = O(1)$, based on the domains, problem interest size. The generated best solution of heat absorber is expressed in Eqn. (30),

$$y_{new} = y_{old} + \in R^t \tag{30}$$

Where, $\in$ denotes the random vector from [-1, 1], R is the average fitness of bat in each iteration. The absorption system's COP is determined as the ratio of absorbed heat by the absorber to the generator's heart rate input is defined in Eqn. (31),

$$COP = \frac{H_a}{H_g} \tag{31}$$

Where, H_g represents the heat rate of the generator. Moreover, the pseudocode of the presented Hybrid Ant Colony Bat Absorber system (HACBAS) is represented in Algorithm 1.

Algorithm: 1 Hybrid Ant Colony Bat Absorber system (HACBAS)

Start
{
Initialization
Int m , $w \Rightarrow Q$
// here Q ***is the input variable***
Designing *CCPP* ***// with HRSG and VAR-based cooling system***
Analyze: *Performance of the designed CCPP*
Develop HACBAS
// combination of ACO and BO
Process of ACO()
Initial stage Process $R^*_{k,l}$ ***// using Eqn. (24)***
Update: *Amount of energy*
// $m_{k,l}$ ***using Eqn. (25)***
Process of BO()
Compute: *Heat absorber velocity increment* H_a ***// fitness of ACO with BO***
Analyze: y_k^{t+1} ***// using Eqn. (29)***
// best heat absorber components
Generate: *Best solution of heat absorber* ***// fitness of BO movement***
// using Eqn. (30)
Compute: y_{new}
Performance analysis ***// developed HACBAS***
Stop
}

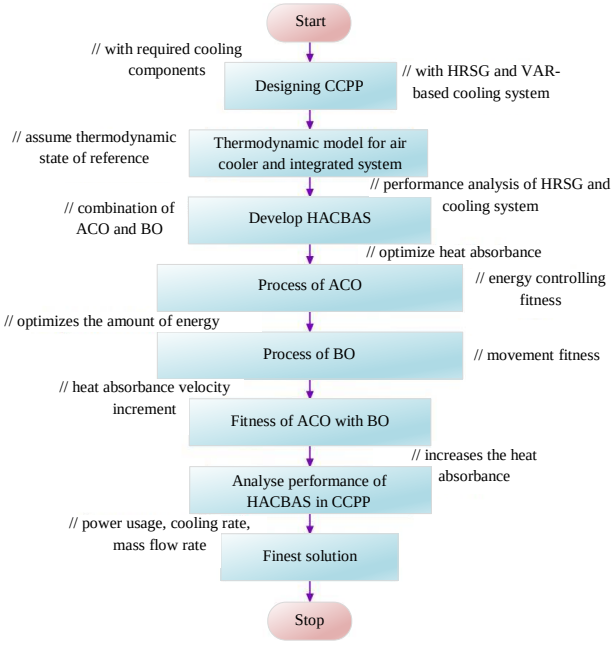

Figure 4 Flowchart of proposed work

Furthermore, the entire process of the proposed HACBAS is explained in the flowchart and represented in Figure 4. Here, the main motive of this work is to optimize the heat absorbance for better cooling capacity and to increase the electricity-producing level by optimizing the amount of energy.

The bat movement changes to obtain the most acceptable outcome at the iteration time. Moreover, the fitness of each bat is evaluated for each iteration. The y_{new}, is considered the best movement of the bat. Consequently, the bat updated its movement and moved through the finest path. The best outcome for the bat is to update its absorbance capacity.

4. Result and discussion

In this section, the proposed method of CCPP with HRSG and VAR-based cooling system is executed in the MATLAB/SIMULINK R2018b running on the Windows 7 platform. It is a restrictive and mathematical programming language developed by Math Works. Moreover, a novel HACBAS is proposed for optimizing heat absorbance. The input parameters of the designed CCPP are tabulated in Table 1.

Table 1 Input parameters of the designed CCPP

Input parameter specification	
Lower-grade thermal energy	80^0C-100^0C
Inlet air	30^0
Ambient air temperature	14^0C-30^0C
AP	5K

4.1 Case study

The CCPP with HRSG and VAR-based cooling system was designed in MATLAB simulation. After the design, a novel HACBAS is implemented to maximize heat absorbance. Moreover, the assumptions taken for integrated CC evaluation [28] are as follows: The thermodynamic state of reference is 1.01325 bar or 101.325 KPa and 25^0C. The gas cycle maximum temperature and pressure ratios are 1200^0C and 8, respectively. Turbine inlets with HP conditions are taken as 600^0C and 200 bars. The difference between superheated steam and flue gas terminal temperature (TTD) is 25 K. HP. The LP economizers approach point (AP) is taken as 15 K, and 0.05 bar is considered for condenser pressure.

The reheat pressure of steam is 50% of high pressure. The pinch point (PP) is described as the minimum difference in temperature between evaporators steam and gas flue is 25 K. The degree of superheat (DSH) is 50 K in a superheater. The GT and compressor efficiency of the isentropic stage is 85%, ST is 90%, the generator's efficiency is 97%, and the combustion chamber's pressure drop is 5%. The AP is 5K in a VAR-based system, and the absorber and condenser's cooling temperatures are taken as 30^0C. HRSG's pressure drop of the condenser and deaerator is neglected. Loss of heat in turbines, deaerator, HRSG, and condenser is ignored. After the process, the performance is validated regarding metrics like power usage, thermal efficiency, cooling rate, ambient temperature, mass flow rate, and relative humidity.

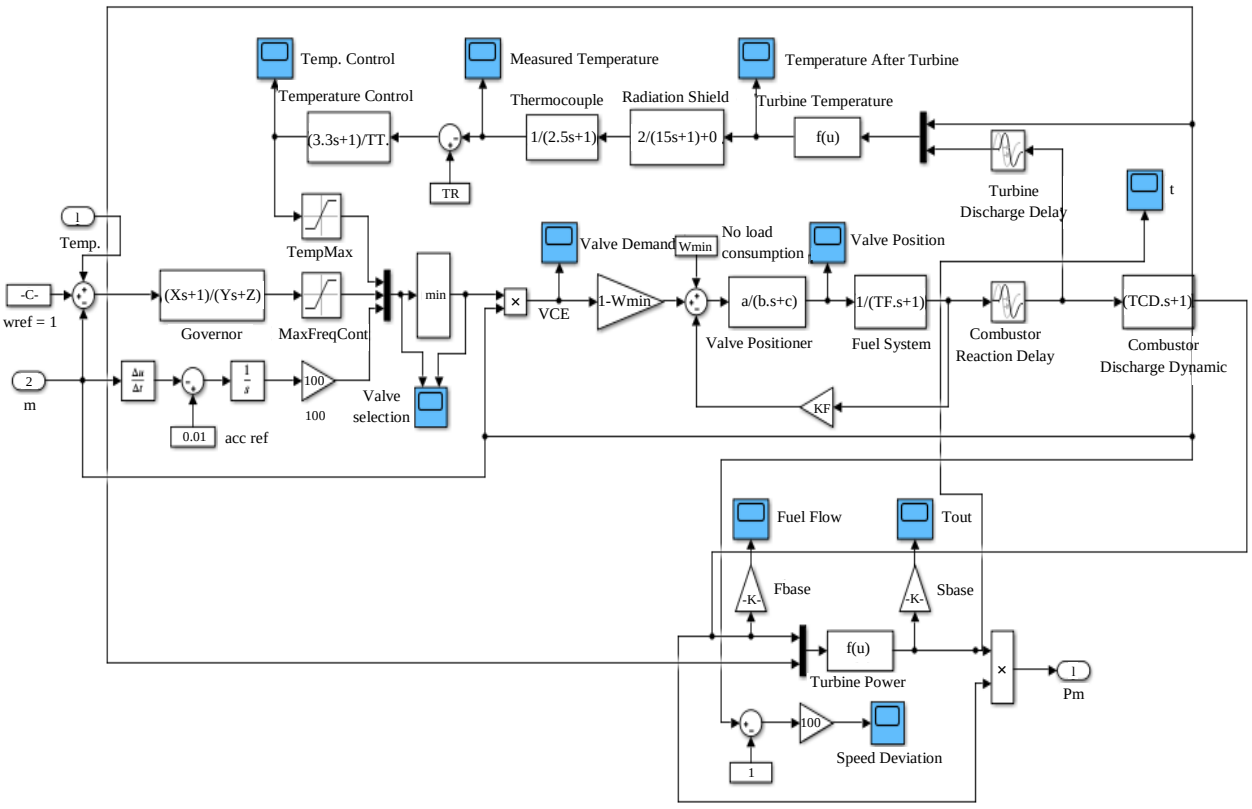

Figure 5 Simulink Gas turbine model

Moreover, the proposed model was implemented under two different temperatures: 15^0C and 25^0C. The temperatures are varied for climate change; as per Nation Climate Report, the average climate change of 2021 is taken and simulated. The simulation diagram of the GT, ST, and HRSG models is shown in Figure 5, Figure 6, and Figure 7, respectively. The compressor map is shown in Figure 8. To measure the compressor stage efficiency performance, the compressor map is drawn. The compressor maps' plots describe the control flow of the designed CCPP.

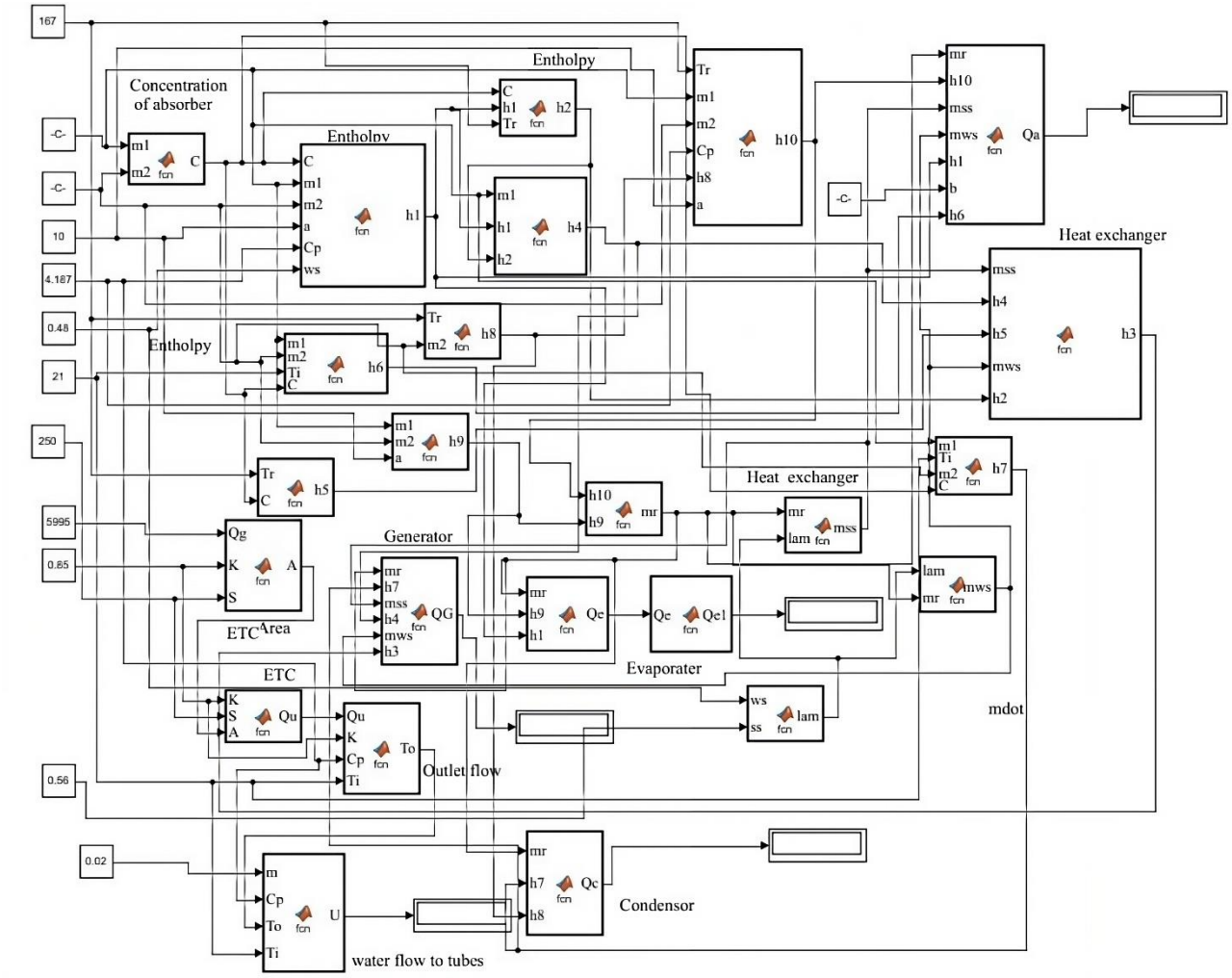

Figure 6 Simulink-HRSG (Cooling plant)

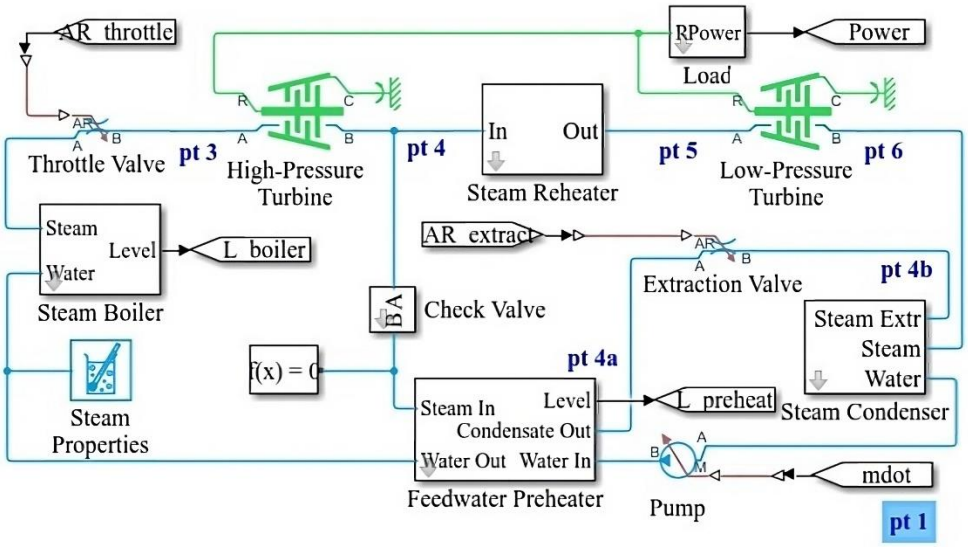

Figure 7 Simulink steam turbine model

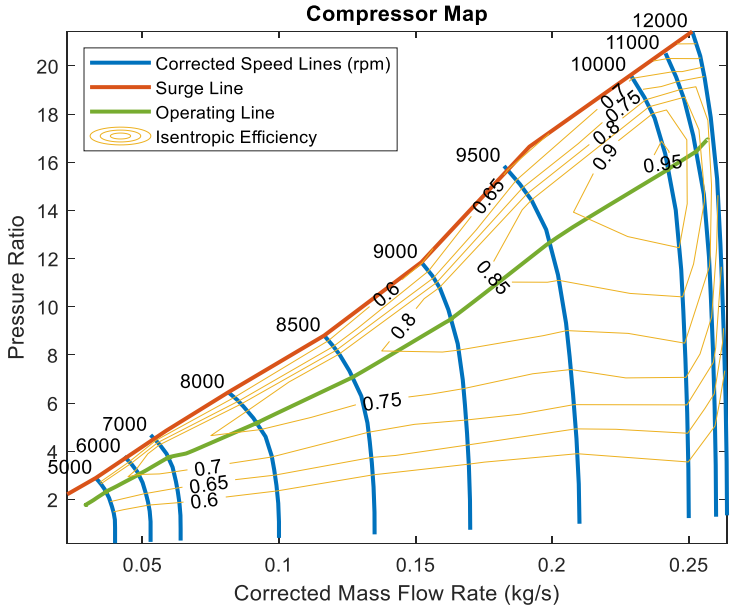

Figure 8 Compressor Map

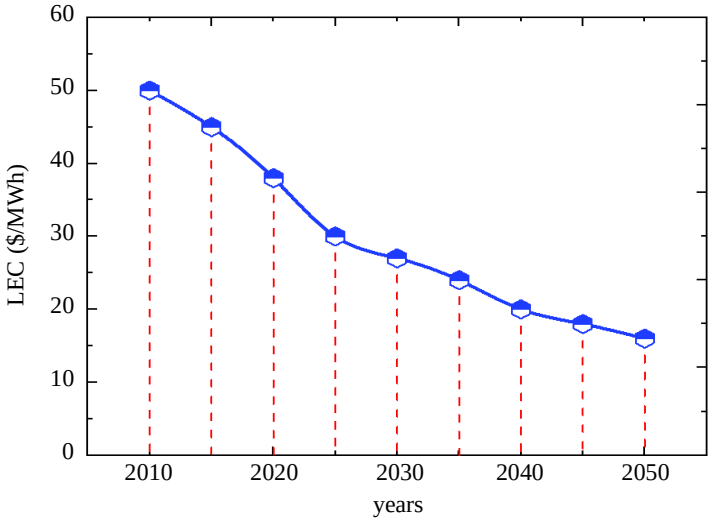

Figure 9 LEC validation

The Levelized Energy-based Cost (LEC) method is utilized to compare the various cases for economic assessment. The lesser LEC is determined as the best choice. Therefore, the investors were calculating the power plant's LEC at first. Moreover, LEC as lower does not mean better efficiency. It is the relationship between cost and efficiency; it led us to the economical choice. In addition, LEC is determined by Eqn. (32),

$$LEC = \frac{V^{*} + \overline{GH} + F_b}{J_{e.out}} \tag{32}$$

Where, V^{*} represents the annual investment cost, $\overline{GH}$ maintenance and operation cost, F_b is the annual cost of fuel, and $J_{e.out}$ is the net amount of gross energy generated (kW/h). Using Eqn. (32), the economic feasibility was determined. Hence, the outcome of the LEC of the designed CCPP system is described in Figure 9.

4.2 Energy flow rate and thermal efficiency

Energy flow rate is defined as the electrical energy per unit of time that flows through a specific time, and it is usually measured in the departments of kilowatts (kW) or Watts (W). The CCPP properties at every state point are shown in Table 2 and Table 3. The plant with lesser power usage is applicable for generating energy. The energy flow rate varies at different times concerning its state points.

Table 2 CCPP properties at 15^0C air temperature at every state point

State point	Fluid	Pressure (bar)	Mass flow rate (kg/s)	Temperature (°C)	Enthalpy (kJ/kg)
1	Steam	200	16.1	350	2908
2	Steam	200	16.1	355	2870
3	Steam	210	16	220	2684
4	Steam	100	16	210	2655
5	Steam	10	15.46	370	2977
6	Steam	9.6	15.46	390	2507
7	Steam	9.6	15.46	390	2507
8	Steam	.05	16.66	15	2339
11	Steam	.05	16.66	15	2289
12	Steam	.05	16.66	15	2289
13	Steam	30	0.1	120	250
14	Steam	62	0.13	179	255
15	Steam	100	0.3	180	260
16	Steam	3.5	9	176	500
17	Steam	3.5	9	178	550
18	Steam	10	15.46	370	2977
19	Steam	10	15.46	370	2977
20	Steam	200	8.1	400	2684
21	Steam	200	8.1	400	2655
22	Steam	8.8	8	400	2685
30	Air	8.8	8	400	2685
31	Air	1.013	551	300	2381
32	Fuel	1.013	551	200	2386
33	Fuel	1.013	113	15.018	777
34	Steam	1.013	113	15.014	440
35	Steam	1.013	113	15.011	435
36	Steam	1.013	113	15.008	398
37	Steam	1.013	113	15.005	957
38	Steam	1.013	113	15.002	352
39	Steam	1.013	113	15	312
40	Steam	1.013	113	15	227
41	Steam	1.013	113	15	181
42	Steam	1.013	113	15	153
43	Steam	1.013	113	15	75.37
44	Steam	1.013	113	15	75.35

Table 3 Cooling plant properties at 15^0C air temperature at each state point

State point	Fluid	Pressure (bar)	Mass flow rate (kg/s)	Temperature (^{0}C)	Enthalpy (kJ/kg)
51	Water	0.654	0.02403	13.5	160
52	Water	0.654	0.02403	13.5	165
53	Exhaust gas	0.654	0.02403	13.5	168
54	Exhaust gas	0.285	0.0245	55	117
55	water	0.285	0.0245	57	176
56	steam	0.285	0.0245	75	175.46
57	steam	0.285	0.0245	140	117
58	Steam	0.285	5	149	170
59	Air	0.654	5	127	155
60	Steam	0.285	5	35	176
61	Steam	0.85	5.001	30	2450.80
62	Steam	0.85	5.655	21	147
63	Steam	0.9	18.02	-37.5	115.30
64	Air	0.9	18.02	-37.5	2606.65
65	Steam	1.01	18.02	-37.5	-31.72

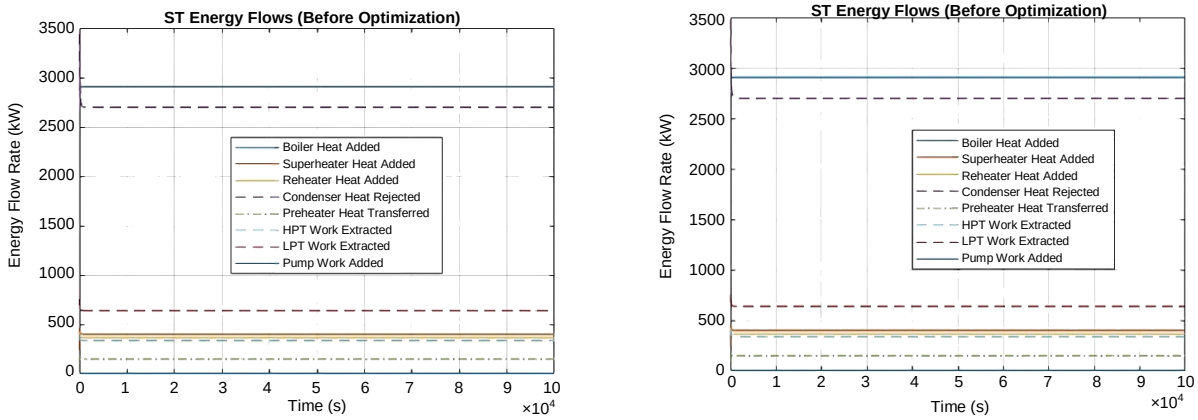

Figure 10 Energy flow rate before optimization (a) 15^0C, (b) 25^0C

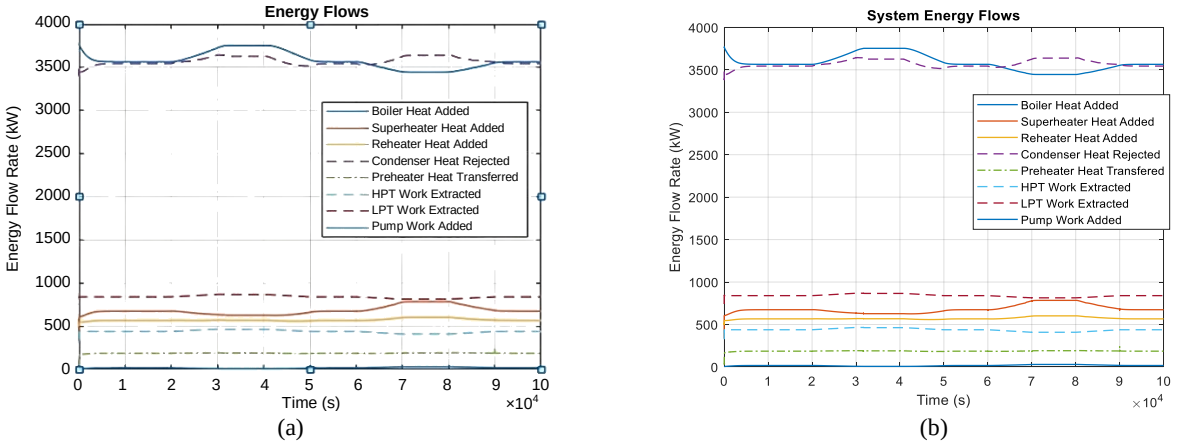

Figure 11 Energy flow rate after optimization (a) at 15^0C (b) at 25^0C

The energy flow rate of the CCPP plat is calculated in dual phases that are before and after applying optimization, which is detailed in Figure 10 and Figure 11. After applying the optimization better energy flow rate has been recorded.

Thermal efficiency is a dimensionless performance measure that utilizes thermal energy, such as the furnace, steam turbine, boiler, refrigerator, and internal-based combustion engine. Based on the thermal efficiency, the pressure-enthalpy has been measured in Figure 12, which is measured by eqn. (33). A heat engine is described as the fraction of primary heat converted into secondary energy (network output). Refrigeration is the ratio of total heat output for heating or removal for cooling to input energy. Moreover, the thermal efficiency obtained in the range of 60-96%; differs for every state point.

$$Enthalpy = initial \quad energy + [\Pr essure \times volume] \tag{33}$$

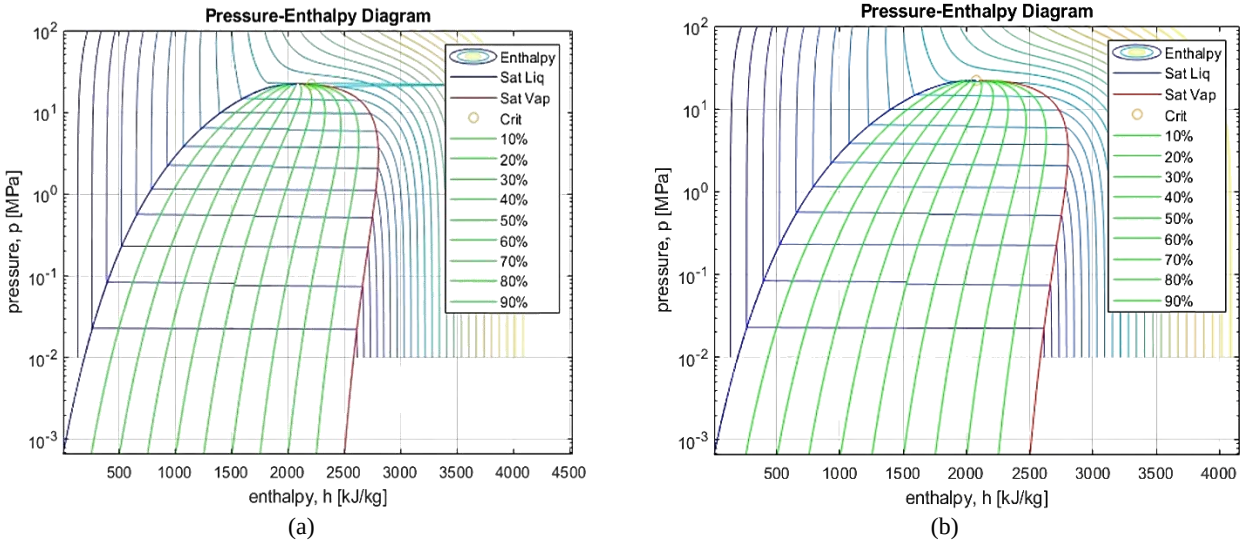

Figure 12 Pressure-Enthalpy (a) at 15^0C (b) at 25^0C

4.3 Cooling rate and mass flow rate

The cooling rate is equivalent to the difference between the two objects' temperatures, multiplied by a constant of the material. The unit of cooling rate is degree/unit-time. The cooling plant properties at each state point are shown in Table 3.

The mass flow rate is the liquid substance mass passing per unit of time. In addition, it is also defined as the movement rate of liquid that passes through a unit area. It directly depends on the liquid velocity, cross-section area, and density. Its unit is kgs-1. Hence, the mass flow rate is measured using eqn. (34).

$$mass \quad flow = \frac{change \quad in \quad mass}{Time} \tag{34}$$

Moreover, the mass flow rate vs. time before applying the hybrid optimization process is shown in Figure 13, and the mass flow rate after applying hybrid optimization is detailed in Figure 14.

The results indicate that plant effectiveness is most significant when the compressor pressure ratio is 8 at a 1,200°C combustion temperature. When the compressor pressure ratio is greater than 10, the cooling method is preferred; when contrasted to the structure without cooling, cooling outcomes of inlet air in high energy output in all equivalence ratios.

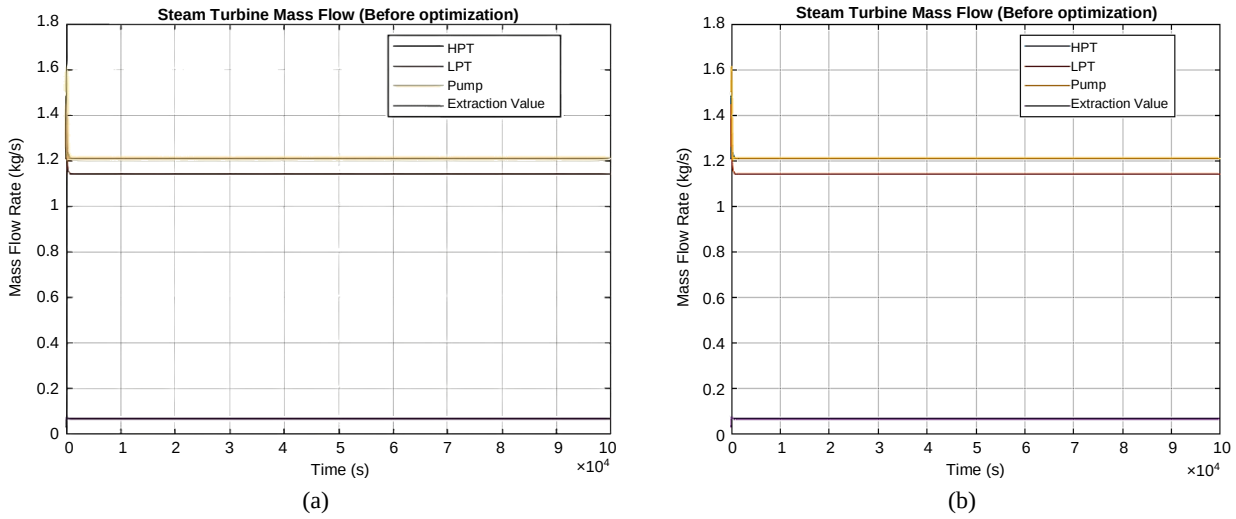

Figure 13 ST mass flow rate before optimization (a) 15^0C, (b) 25^0C

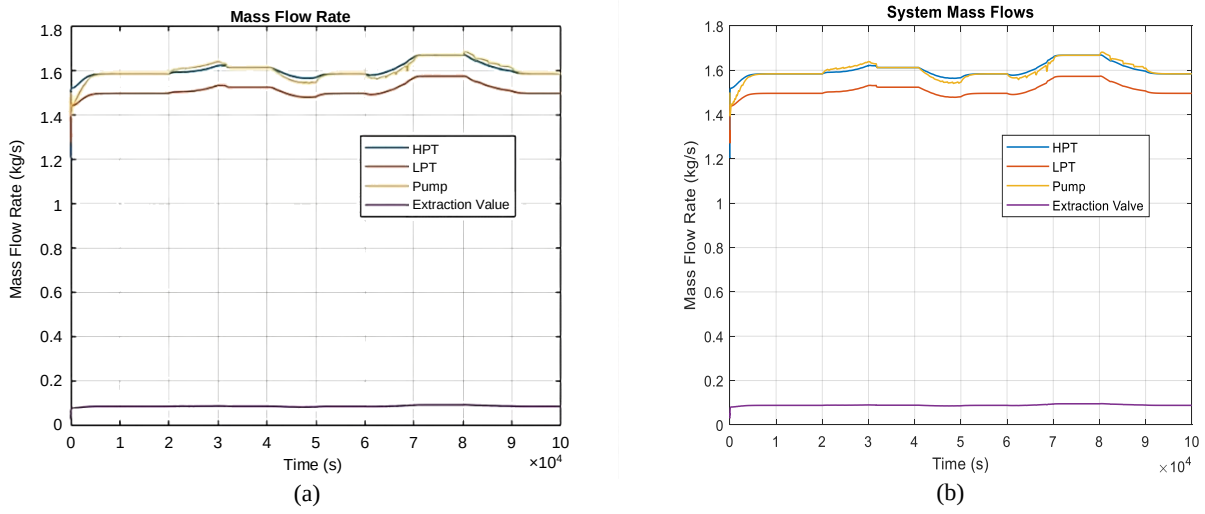

Figure 14 ST Mass flow rate after optimization (a) at 15^0C (b) at 25^0C

4.4 Ambient temperature and relative humidity

The CCPP performance was firmly based on the ambient temperature. It is defined as the environment or object air temperature of equipment is stored. Moreover, when the ambient temperature rises, the total power generated in the CCPP decreases, and the heat increases, i.e., decreases efficiency.

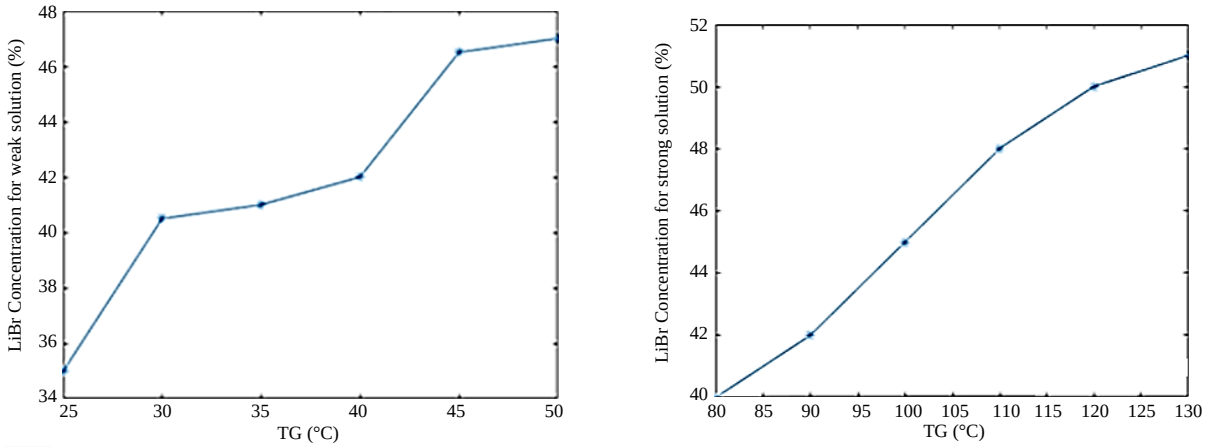

Figure 15 LiBr concentration (a) weak solution (b) strong solution

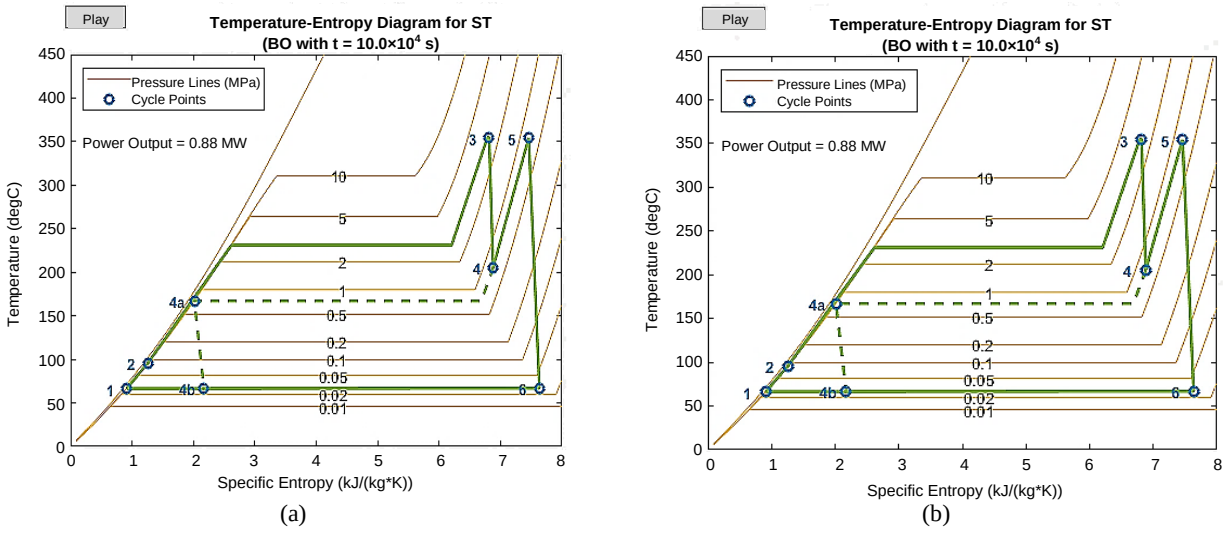

Figure 16 Temperature vs Entropy Before optimization (BO) (a) at 15^0C (b) at 25^0C

The Lithium Bromide (LiBr) concentration for both weak and strong solutions is shown in Figure 15. The graph of temperature vs entropy before applying the fitness of hybrid optimization is shown in Figure 16, and the entropy results after applying the optimization function are described in Figure 17. The compressor's inlet air temperature differs from 14°C to 30°C, and the compressor pressure ratio changes from 7 to 16. Even without air cooling, the air is conceded at 30°C, implying that the air coolant is circumvented. Moreover, the ambient temperature is 12-33^0C for the developed CCPP.

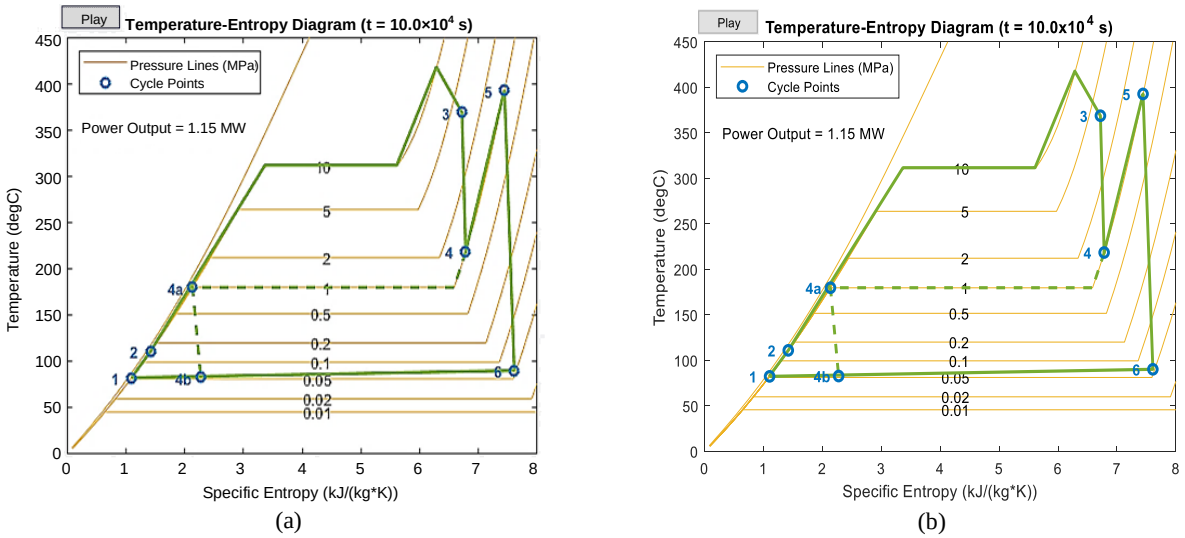

Figure 17 Temperature vs Entropy after optimization: (a) at 15^0C (b) at 25^0C

The relative humidity is the ratio of total water vapor in the air to the most significant amount at the same temperature. Its unit is %, also described as the ratio between the moisture amounts in the air at a particular temperature to the maximum moisturized air can withstand at the same temperature. The relative humidity obtained by the presented approach is 50% and 100%.

4.5 Comparative analysis of Coefficient of performance (COP)

The Coefficient of performance (COP) measures the amount of heat energy moved compared to use heat energy. Moreover, the presented model has attained a COP of 0.97. Further, to identify the effectiveness of the proposed method, the COP was compared with existing techniques like automated MPFHE [29] and Renewable CCPP [30]. Furthermore, the obtained COP for the presented model is shown in Figure 18. Here, the green line indicates the performance of the conventional CCPP, and the blue line represents the Optimized CCPP.

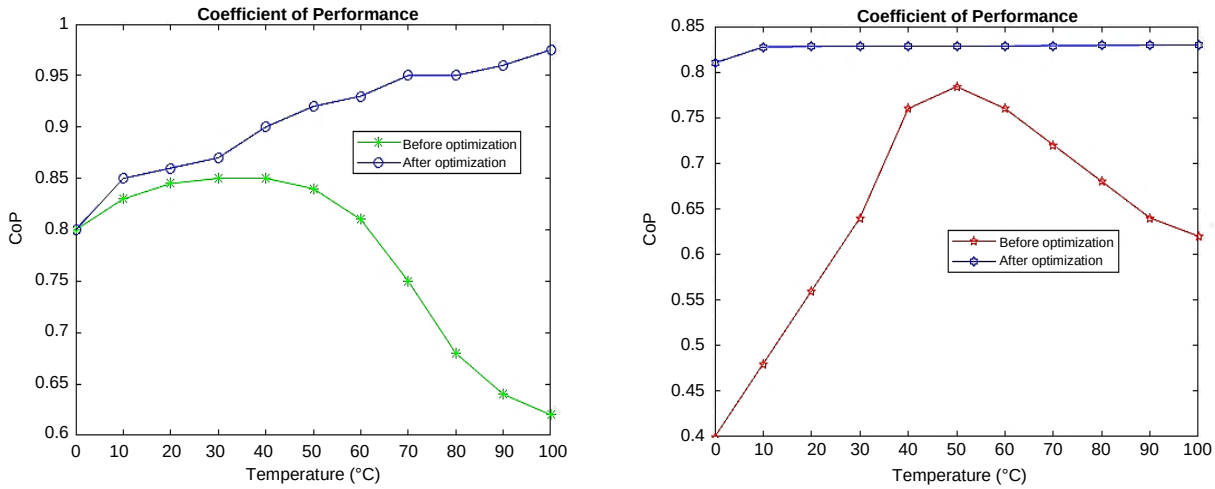

Figure 18 Obtained COP (a) at 15^0C (b) at 25^0C

Table 4 Coefficient of performance comparison

Sl.no	Technique		Coefficient of performance
1	Automated MPHFE [29]		0.694
2	Renewable CCPP [30]		0.56
3	Proposed	Before optimization	0.45
		After optimization	0.97

By comparing with other models, the presented model has attained higher COP. To get the exactness improvement of COP, the existing models like Automated MPHFE and renewable CCPP are implemented in the same platform. Hence, it has shown a reduced COP than the proposed model. Moreover, the average of the COP is taken based on the given input energy and produced output energy or power. Hence, the statistics are defined in Table 4. The automated MPHE has earned a COP of 0.694, and the renewable CCPP has attained a COP of 0.56. The given thermophysical properties increase the exit temperature and drop the COP for working fluid more than other models.

4.6 Discussion

Several traditional methods are explained, and their outcomes are compared with other models. Hence, this state-of-the-art has helped to identify future work by identifying the demerits of the current position. The demerits and merits of the existing model are described in Table 5.

Table 5 State-of-art comparison

Author name	Technique	Merits	Demerits
Gado et al. [19]	Hybrid sorption-vapor and compression cooling system	Accurate temperature with high-speed response, suitable for humid and hot temperature	Lack of moving parts and more time are introduced into the market.
Alklaibi and Lior [20]	ARS	Fuel consumption is reduced by 5-11.3%; thermal efficiency is increased up to 5%	Improved 3% heat recovery
Peng and Sadaghiani [21]	Integrated Cooling System	Exergy efficiency rate is high	Optimization increase of the capital costs
Fakhari et al. [22]	Combined energy analysis	High energy efficiency and power-producing level	Exergy destruction happened during the process
Proposed	HACBAS	High Coefficient of performance, heat-producing capacity, and attained best cooling capacity.	-

Moreover, the proposed method has less cost because CCPP was designed in the MATLAB environment. In addition, it reduces the energy consumption of other CCPPs.

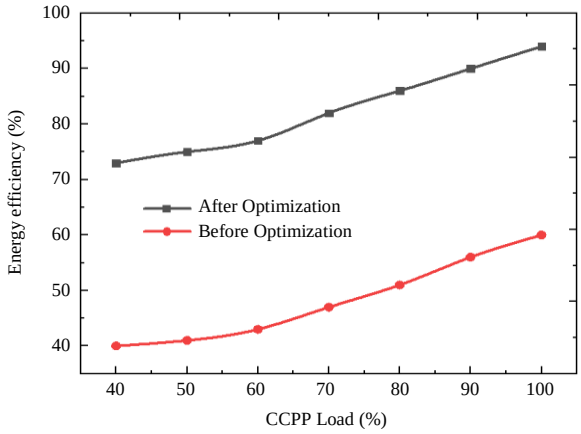

Figure 19 Comparison of energy efficiency

The main cause of desired power generation is improving energy efficiency. Hence, the energy efficiency has been calculated and compared with conventional methods with different loads, which is graphically described in Figure 19.

The main motive for designing this optimized CCPP has produced the desired power. Hence, the power generation output has been calculated for the designed novel HACBAS CCPP. To show the need for optimization for the CCPP, the power generation output is measured for conventional CCPP, described before optimization in Figure 20.

In addition, if the steam temperature was maximized, the power output decreased considerably. Hence, the fall of the power output has been measured in dual phases before and after applying the optimization approach described in Figure 21. However, the proposed CCPP system has gained the finest outcome after applying the optimization model. Before optimization, at 200^0C, the power was decreased. After optimization, the power was decreased at the point of 220^0C. This has verified the efficiency of the present CCPP system.

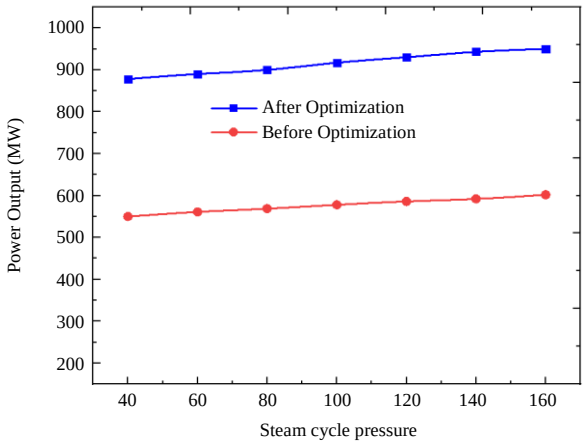

Figure 20 Comparison of Power generation

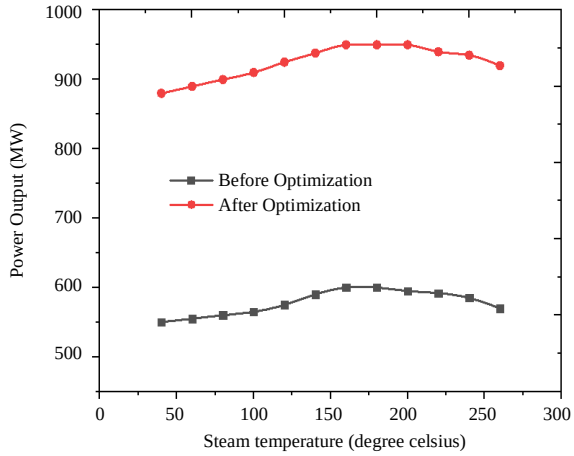

Figure 21 Power fall output

5. Conclusion

In this study, the Combined Cycle Power Plant (CCPP) with HRSG and VAR-based cooling system is designed in MATLAB simulation. A single-effect-based Lithium Bromide-water ($LiBr/H_2O$) VAR cooling system was created using a thermodynamic process. Moreover, the heat absorbance was optimized by developing the Hybrid Ant Colony Bat Absorber System (HACBAS). Consequently, the absorption system is most suitable for CCPP. The system's performance is validated by power usage, ambient temperature, relative humidity, thermal efficiency, mass flow rate, and cooling rate. Compared with the existing CCPPs with cooling systems, the system efficiency has gained the most acceptable CCPP efficiency rate. Before applying the hybrid optimization, the normal CCPP achieved a low COP rate of 0.45. After applying the Hybrid optimization, the COP has improved to 0.97. Compared to the conventional CCPP, the Optimized CCPP has improved the COP by 5%. Also, the energy efficiency of the traditional CCPP is 60%, and after applying the hybrid optimization, the energy efficiency has been maximized to 95%. It has proven a 35% improvement in energy efficiency rate. In the future, designing the emission analyzing and controlling model will enhance CCPP performance.

6. References

[1] Dokhaee E, Saraei A, Mohsenimonfared H, Yousefi P. Exergy and thermoeconomic analysis of a combined Allam generation system and absorption cooling system. Int J Energy Environ Eng. 2022;13:267-73.

[2] Nazarzadehfard A, Saraei A, Jafari Mehrabadi S, Mohsenimonfared H. Exergy and thermoeconomic analysis of the combined MED desalination system and the Allam power generation system. Int J Energy Environ Eng. 2021;12:679-87.

[3] Enteria N, Cuartero-Enteria O, Sawachi T. Review of the advances and applications of variable refrigerant flow heating, ventilating, and air-conditioning systems for improving indoor thermal comfort and air quality. Int J Energy Environ Eng. 2020;11:459-83.

[4] Meli K, Koliopoulos D, Lavidas K. A model-based constructivist approach for bridging qualitative and quantitative aspects in teaching and learning the first law of thermodynamics. Sci Educ. 2022;31:451-85.

[5] Rohli RV, Li C. Energy Transfer and Electromagnetic Radiation. In: Meteorology for Coastal Scientists. Cham: Springer; 2021. p. 27-47.

[6] Aminov RZ, Bayramov AN. Current state and prospects of hydrogen production at NPPs. Therm Eng. 2021;68(9):663-672.

[7] Qu Z, Xu J, Wang Z, Chi R, Liu H. Prediction of electricity generation from a combined cycle power plant based on a stacking ensemble and its hyperparameter optimization with a grid-search method. Energy. 2021;227:120309.

[8] Köse Ö, Koç Y, Yağl, H. Energy, exergy, economy and environmental (4E) analysis and optimization of single, dual and triple configurations of the power systems: Rankine Cycle/Kalina Cycle, driven by a gas turbine. Energy Convers Manag. 2021;227:113604.

[9] Wang X, Xu Y, Bao Z, Li W, Liu F, Jiang Y. Operation optimization of a solar hybrid CCHP system for adaptation to climate change. Energy Convers Manag. 2020;220:113010.

[10] Madadian E, Haelssig JB, Mohebbi M, Pegg M. From biorefinery landfills towards a sustainable circular bioeconomy: A techno-economic and environmental analysis in Atlantic Canada. J Clean Prod. 2021;296:126590.

[11] Li J, Zoghi M, Zhao L. Thermo-economic assessment and optimization of a geothermal-driven tri-generation system for power, cooling, and hydrogen production. Energy. 2022;244:123151.

[12] Ferry J, Widyolar B, Jiang L, Winston R. Solar thermal wastewater evaporation for brine management and low pressure steam using the XCPC. Appl Energy. 2020;265:114746.

[13] Jiang L, Gonzalez-Diaz A, Ling-Chin J, Roskilly AP, Smallbone AJ. Post-combustion CO_2 capture from a natural gas combined cycle power plant using activated carbon adsorption. Appl Energy. 2019;245:1-15.

[14] Mohammadi K, Ellingwood K, Powell K. A novel triple power cycle featuring a gas turbine cycle with supercritical carbon dioxide and organic rankine cycles: thermoeconomic analysis and optimization. Energy Convers Manag. 2020;220:113123.

[15] Arabkoohsar A. Combination of air-based high-temperature heat and power storage system with an organic rankine cycle for an improved electricity efficiency. Appl Therm Eng. 2020;167:114762.

[16] Salehi M, Eivazi H, Tahani M, Masdari M. Analysis and prediction of gas turbine performance with evaporative cooling processes by developing a stage stacking algorithm. J Clean Prod. 2020;277:122666.

[17] Karatas Y, Yilmaz D. Experimental investigation of the microclimate effects on floating solar power plant energy efficiency. Clean Technol Environ Policy. 2021;23:2157-70.

[18] Deng C, Al-Sammarraie AT, Ibrahim TK, Kosari E, Basrawi F, Ismail FB, et al. Air cooling techniques and corresponding impacts on combined cycle power plant (CCPP) performance: a review. Int J Refrig. 2020;120:161-77.

[19] Gado MG, Ookawara S, Nada S, El-Sharkawy II. Hybrid sorption-vapor compression cooling systems: a comprehensive overview. Renew Sust Energ Rev. 2021;143:110912.

[20] Alklaibi AM, Lior N. Waste heat utilization from internal combustion engines for power augmentation and refrigeration. Renew Sust Energ Rev. 2021;152:111629.

[21] Peng W, Sadaghiani OK. Presentation of an integrated cooling system for enhancement of cooling capability in Heller cooling tower with thermodynamic analyses and optimization. Int J Refrig. 2021;131:786-802.

[22] Fakhari I, Behinfar P, Raymand F, Azad A, Ahmadi P, Houshfar E, et al. 4E analysis and tri-objective optimization of a triple-pressure combined cycle power plant with combustion chamber steam injection to control NOx emission. J Therm Anal Calorim. 2021;145(3):1317-33.

[23] Sazal Miah M, Bhowmick SK, Rezaul Karim Sohel M, Abdul Momen Swazal M, Mittro S, Hossain Lipu MS. Feasibility study of combined cycle power plant in context of bangladesh. In: In: Raj JS, Palanisamy R, Perikos I, Shi Y, editors. Intelligent sustainable systems. Singapore: Springer; 2022. p. 447-64.

[24] Wan A, Yang J, Chen T, Huang J. Techno-economic analysis of combined cycle power plant with waste heat-driven adsorption inlet air cooling system. Int Commun Heat Mass Transf. 2021;126:105422.

[25] Ahmad AD, Abubaker AM, Najjar YSH, Manaserh YMA. Power boosting of a combined cycle power plant in Jordan: an integration of hybrid inlet cooling & solar systems. Energy Convers Manag. 2020;214:112894.

[26] Christy Jeba Malar A, Kowsigan M, Krishnamoorthy N, Karthick S, Prabhu E, Venkatachalam K. Multi constraints applied

energy efficient routing technique based on ant colony optimization used for disaster resilient location detection in mobile ad-hoc network. J Ambient Intell Human Comput. 2020;12(3):4007-17. Retraction in: J Ambient Intell Human Comput. 2023;14:495.
[27] Cao Y, Dhahad HA, Farouk N, Xia WF, Rad HN, Ghasemi A, et al. Multi-objective bat optimization for a biomass gasifier integrated energy system based on 4E analyses. Appl Therm Eng. 2021;196:117339.
[28] Srinivas T, Vignesh D. Performance enhancement of GT-ST power plant with inlet air cooling using lithium bromide/water vapour absorption refrigeration system. Int J Energy Technol Policy. 2012;8(1):94-107.
[29] Allahyarzadeh-Bidgoli A, Dezan DJ, Yanagihara JI. COP optimization of propane pre-cooling cycle by optimal Fin design of heat exchangers: efficiency and sustainability improvement. J Clean Prod. 2020;271:122585.
[30] Seyam S, Dincer I, Agelin-Chaab M. Development of a clean power plant integrated with a solar farm for a sustainable community. Energy Convers Manag. 2020;225:113434.